Scanning tunneling potentiometry, charge transport, and Landauer's resistivity dipole from the quantum to the classical transport regime

Dirk K. Morr
University of Illinois at Chicago, Chicago, Illinois 60607, USA
(Received 27 January 2017; published 30 May 2017)

Using the nonequilibrium Keldysh formalism, we investigate the spatial relation between the electrochemical potential measured in scanning tunneling potentiometry, and local current patterns over the entire range from the quantum to the classical transport regime. These quantities show similar spatial patterns near the quantum limit but are related by Ohm's law only in the classical regime. We demonstrate that defects induce a Landauer residual resistivity dipole in the electrochemical potential with the concomitant spatial current pattern representing the field lines of the dipole.

DOI: 10.1103/PhysRevB.95.195162

I. INTRODUCTION

Visualizing charge transport at the nanoscale is not only of great fundamental interest to understand and explore the crossover from quantum to classical transport, but also important for the continued miniaturization of electronic circuits. While spatial imaging of charge currents at the mesoscale has been achieved using scanning probe microscopy [1–10], scanning tunneling potentiometry [11–14] (STP) [see Fig. 1(a)] has been employed to gain insight into the nature of charge transport at much smaller length scales down to the nanometer scale [15–18]. This has led to the observation of Landauer's residual resistivity dipoles [19,20] near step edges [15,17,18]. The question, however, arises as to whether one can gain direct insight into the spatial form of the current density—or, more generally, the current patterns—from the electrochemical potential. While in the limit of classical, diffusive transport the relation between these two quantities is established by Ohm's law, most materials of interest possess sufficiently long mean free paths such that they lie between the classical and quantum transport limits. In this regime, the relation between the local electrochemical potential and the current density is unknown, and identifying it is therefore crucial for visualizing the spatial flow of currents at the nanometer scale.

In this article, we provide this missing link by identifying the relation between the spatial form of the electrochemical potential $\mu_e(\mathbf{r})$ as determined via STP and the spatial current pattern $I_{\mathbf{r},\mathbf{r}'}$ over the entire range from the quantum to the classical transport regime. Using the Keldysh Green's function formalism [21–23], we demonstrate that near the quantum limit, the spatial form of $\mu_e(\mathbf{r})$ is similar to that of $I_{\mathbf{r},\mathbf{r}'}$, such that the electrochemical potential can be employed to spatially image the current pattern. On the other hand, we show that Ohm's law can only be used in the classical limit to directly deduce the local current density $I_{\mathbf{r},\mathbf{r}'}$ from the spatial form of $\mu_e(\mathbf{r})$. Moreover, we demonstrate that the evolution of $\mu_e(\mathbf{r})$ between the quantum and classical limit is reflected in changes of an effective Fermi distribution function. We show that defects induce a Landauer's residual resistivity dipole in $\mu_e(\mathbf{r})$ and that the concomitant spatial form of $I_{\mathbf{r},\mathbf{r}'}$ is that of field lines associated with the presence of a dipole. Finally, we demonstrate that $\mu_e(\mathbf{r})$ changes sharply at interfaces or step edges accompanied by large-scale spatial oscillations. These results identify the relation between the electrochemical potential and the local flow of charges over the entire range from quantum to classical transport.

II. THEORETICAL FORMALISM

To investigate the form of the local electrochemical potential $\mu_e(\mathbf{r})$, its relation to the spatial current pattern, and its evolution from the quantum to the classical limit, we consider a network of electronic sites that are connected by hopping elements as shown in Fig. 1(b) [24–29]. These sites can represent atoms, molecules, or quantum dots; for the present purpose we assume that they possess only a single electronic level. The network is coupled to two leads and described by the Hamiltonian $H = H_0 + H_{\rm def} + H_{\rm ph} + H_c + H_{\rm tun} + H_{\rm tip} + H_{\rm lead}$, where

$$\begin{aligned} H_0 &= \sum_{\mathbf{r},\mathbf{r}',\sigma} (-t - \mu\delta_{\mathbf{r},\mathbf{r}'}) c^\dagger_{\mathbf{r}\sigma} c_{\mathbf{r}'\sigma} \\ H_{\rm def} &= U_0 \sum_{\mathbf{R},\sigma} c^\dagger_{\mathbf{R},\sigma} c_{\mathbf{R},\sigma} \\ H_{\rm ph} &= g \sum_{\mathbf{r},\sigma} c^\dagger_{\mathbf{r}\sigma} c_{\mathbf{r}\sigma} (a^\dagger_{\mathbf{r}} + a_{\mathbf{r}}) + \omega_0 \sum_{\mathbf{r},\sigma} a^\dagger_{\mathbf{r}} a_{\mathbf{r}} \\ H_c &= -t_c \sum_{j,\sigma} \left(c^\dagger_{\mathbf{R}_j,\sigma} d_{\mathbf{R}_j,\sigma} + c^\dagger_{\mathbf{L}_j,\sigma} d_{\mathbf{L}_j,\sigma} + \text{H.c.} \right) \\ H_{\rm tun} &= -t_{\rm tip} \sum_{\sigma} (c^\dagger_{\mathbf{r}\sigma} f_\sigma + f^\dagger_\sigma c_{\mathbf{r}\sigma}). \end{aligned} \tag{1}$$

Here, $c^\dagger_{\mathbf{r}\sigma}(c_{\mathbf{r}'\sigma})$ creates (annihilates) an electron with spin σ at site $\mathbf{r}$ in the network, $-t$ is the electronic hopping between nearest-neighbor sites, and μ is the chemical potential. $H_{\rm def}$ describes the electronic scattering off nonmagnetic defects located at sites $\mathbf{R}$, and $H_{\rm ph}$ represents the interaction of the electrons with local Einstein phonon modes of energy ω_0. H_c describes the coupling of the network to the left and right leads, and $H_{\rm tun}$ represents the tunneling of an electron from the tip to a site $\mathbf{r}$ in the network. Finally, $H_{\rm tip}$ and $H_{\rm lead}$ describe the electronic structure of the tip and the leads, respectively. Below, we assume the wide-band limit for both with a constant density of states $N_0 = 1/t$. Moreover, we set $\mu = 0$, yielding the Fermi surface shown in the inset of Fig. 1(c). We had previously shown [29] that by increasing g, one can tune

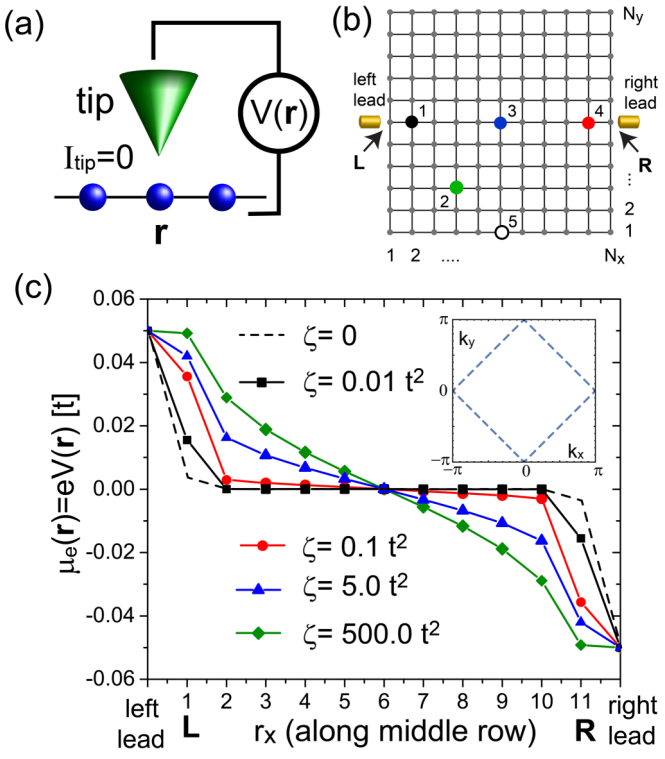

FIG. 1. (a) Schematic representation of STP: when the STP tip is above at site $\mathbf{r}$ of the network, its potential $V(\mathbf{r})$ is adjusted such that there is a zero net current flowing between the tip and the network. (b) Network of electronic sites that are connected by electronic hopping (solid black lines) and coupled to two narrow leads. (c) $\mu(\mathbf{r})$ along the middle row of the network in (b) for different values of ζ. Inset: Fermi surface of the network.

the network's transport properties from the quantum to the classical limit. Here, the quantum limit, $g = 0$, describes a fully coherent system with an infinitely large elastic mean free path, $\xi = \infty$, while the classical limit is obtained for $g \to \infty$ with $\xi \approx a_0$ (a_0 is the lattice constant). To investigate the crossover from quantum to classical transport, we employ the high-temperature approximation $k_B T \gg \hbar\omega_0$ [29,30], where the strength of the electron-phonon interaction is characterized by a single parameter, $\zeta = 2g^2 k_B T/(\hbar\omega_0)$, with $\zeta = 0$ and $\zeta \to \infty$ corresponding to the quantum and classical transport limits, respectively.

When different chemical potentials $\mu_{L,R}$ are applied to the left and right leads, a nonzero current flows through the network. The resulting spatial current pattern $I_{\mathbf{r},\mathbf{r}'}$ inside the network can be computed using the nonequilibrium Keldysh Green's function formalism [21–23,29]. At the same time, the current between the STP tip and a site $\mathbf{r}$ in the network in the weak tunneling limit is given by [28]

$$I_{\rm tip}(\mathbf{r}) = -2\frac{g_s e}{\hbar} N_0 t_{\rm tip}^2 \int_{-\infty}^{\infty} \frac{d\omega}{2\pi} \left\{ \frac{{\rm Im}G^<(\mathbf{r},\mathbf{r},\omega)}{2} + n_F^{\rm tip}[\omega - eV(\mathbf{r})]{\rm Im}G^r(\mathbf{r},\mathbf{r},\omega) \right\}, \quad (2)$$

where $G^{<,r}(\mathbf{r},\mathbf{r},\omega)$ are the full local lesser and retarded Green's functions, $n_F^{\rm tip}$ is the Fermi distribution function of the tip, and $V(\mathbf{r})$ is the potential in the tip with respect to the network (for a detailed discussion of $G^<(\mathbf{r},\mathbf{r},\omega)$, see Ref. [29]). To obtain the electrochemical potential, $\mu_e(\mathbf{r}) = eV(\mathbf{r})$ via STP, $V(\mathbf{r})$ is adjusted at every site $\mathbf{r}$ such that $I_{\rm tip}(\mathbf{r}) = 0$.

III. RESULTS

In Fig. 1(c), we present the evolution of $\mu_e(\mathbf{r})$ along the center row of the network in Fig. 1(b) with increasing ζ. In the noninteracting quantum limit, $\zeta = 0$, the chemical potential abruptly changes at the lead-network interface and is nearly constant inside the network. This interface resistance limits the network's conductance to the quantum of conductance [29]. With increasing ζ, the resulting electronic dephasing leads not only to a varying $\mu_e(\mathbf{r})$ inside the network, but also to an evolution in its spatial form, as shown in Figs. 2(a)–2(c). To investigate the relation between $\mu_e(\mathbf{r})$ and the corresponding spatial current pattern, $I_{\mathbf{r},\mathbf{r}'}$, we plot the latter in Figs. 2(d)–2(f) (for details of its calculation, see Ref. [29]). For large ζ, the spatial forms of $\mu_e(\mathbf{r})$ [Fig. 2(c) for $\zeta = 500t^2$] and of $I_{\mathbf{r},\mathbf{r}'}$ are that of a classical resistor network [31], for which $\mu_e(\mathbf{r})$ is shown in Fig. 2(g). In this case, $\mu_e(\mathbf{r})$ and $I_{\mathbf{r},\mathbf{r}'}$ (both obtained within the Keldysh formalism) are related by Ohm's law, $I_{\mathbf{r},\mathbf{r}'} = \sigma(\mathbf{r},\mathbf{r}')[\mu_e(\mathbf{r}) - \mu_e(\mathbf{r}')]$, with the link conductivity between two neighboring sites being constant, i.e., $\sigma(\mathbf{r},\mathbf{r}') = \sigma_0$. In the opposite limit of small ζ, i.e., near the quantum limit, $\mu_e(\mathbf{r})$ [Fig. 2(a)] shows a spatial form that is very similar to that of $I_{\mathbf{r},\mathbf{r}'}$ [Fig. 2(d)], implying that $\mu_e(\mathbf{r})$ can be used to spatially image regions of large current density. However, neither in this limit, nor in the crossover region between quantum and classical transport [as exemplified by $\zeta = 0.5t^2$, Figs. 2(b) and 2(e)] are $\mu_e(\mathbf{r})$ and $I_{\mathbf{r},\mathbf{r}'}$ related by Ohm's law with a constant σ_0. To demonstrate this, we present in Fig. 2(h) a spatial plot of $I_{\mathbf{r},\mathbf{r}'}$ obtained from $\mu_e(\mathbf{r})$ in Fig. 2(b) [for intermediate $\zeta = 0.5t^2$] using Ohm's law with a constant σ_0. Not only does the resulting $I_{\mathbf{r},\mathbf{r}'}$ not obey the continuity equation, but its spatial form is also qualitatively different from that of the actual current pattern shown in Fig. 2(e). We therefore conclude that the spatial current pattern $I_{\mathbf{r},\mathbf{r}'}$ can only be extracted from $\mu_e(\mathbf{r})$ via Ohm's law in the classical transport regime.

Further insight into the nature of the local potential can be gained by considering a graphical solution of the condition $I_{\rm tip}(\mathbf{r}) = 0$ from Eq. (2). To this end, we present in Fig. 3(a) a plot of ${\rm Im}G^{<,r}$ for site 5 in Fig. 1(b) and $\zeta = 0.1t^2$. A closer analysis of Eq. (2) reveals that $V(\mathbf{r})$ (for which $I_{\rm tip}(\mathbf{r}) = 0$) is determined by the condition that the area between $-{\rm Im}G^r$ and ${\rm Im}G^</2$ for $\mu_R < \omega < eV(\mathbf{r})$ (blue area) be equal to the area under ${\rm Im}G^</2$ for $eV(\mathbf{r}) < \omega < \mu_L$ (green area). To provide a physical interpretation of this result, we define an effective out-of-equilibrium Fermi distribution function $\bar{n}_F$ in the network via $G^<(\mathbf{r},\mathbf{r},\omega) = -2i\bar{n}_F(\omega){\rm Im}G^r(\mathbf{r},\omega)$. In equilibrium, $\bar{n}_F$ is the conventional Fermi distribution function. In Fig. 3(b) we present $\bar{n}_F$ at sites 1–4 in Fig. 1(b) for small $\zeta = 0.01t^2$, together with $n_F^{\rm tip}$. As the network is out of equilibrium, $\bar{n}_F$ is modified from its equilibrium form in the energy range $\mu_R < \omega < \mu_L$ and varies greatly inside the network. For $\mu_R < \omega < eV(\mathbf{r})$, $n_F^{\rm tip} = 1 > \bar{n}_F$, and these states carry a current from the tip into the network. On the other hand, for $eV(\mathbf{r}) < \omega < \mu_L$, one has $n_F^{\rm tip} = 0 < \bar{n}_F$, and hence these states carry a current that flows from the

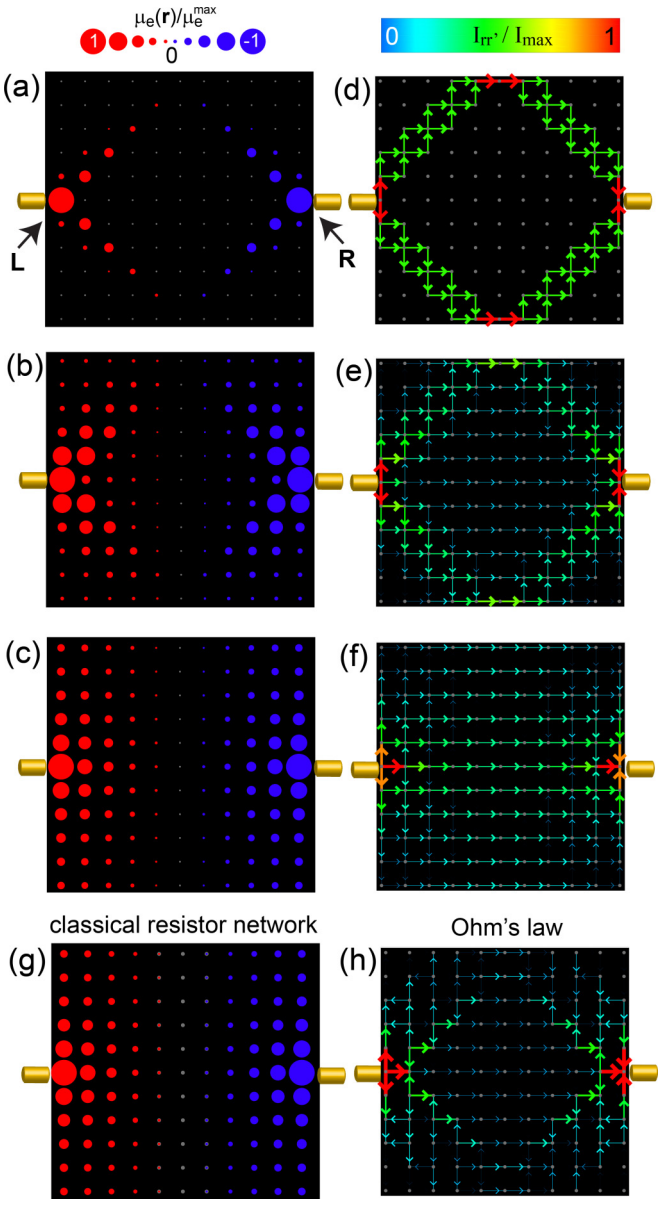

FIG. 2. Network with $N_x = N_y = 11$: normalized $\mu_e(\mathbf{r})/\mu_e^{\max}$ for (a) $\zeta = 0.01t^2$, (b) $\zeta = 0.5t^2$, and (c) $\zeta = 500t^2$, and (c)–(e) corresponding normalized current pattern $I_{\mathbf{r},\mathbf{r}'}/I_{\max}$ for $T = 0$, $t_c = t$, and $\mu_{L,R} = \pm 0.05t$. (g) $\mu_e(\mathbf{r})$ in a classical resistor network connected to two narrow leads. (h) $I_{\mathbf{r},\mathbf{r}'}$ obtained from (b) using Ohm's law with constant σ_0. $\mu_e(\mathbf{r})$ at sites $\mathbf{L},\mathbf{R}$ in (a) and (b) has been divided by a factor of 15 and 4, respectively, for clarity.

network into the tip. For an appropriately chosen $V(\mathbf{r})$, these two counterpropagating currents [as represented by the blue and green areas in Fig. 3(a)] cancel such that $I_{\text{tip}}(\mathbf{r}) = 0$, as previously also pointed out in Ref. [28]. Moreover, while $\bar{n}_F$ exhibits a strong energy dependence between μ_L and μ_R for small ζ, this dependence becomes weaker with increasing ζ, until $\bar{n}_F(\mathbf{r},\omega) = \bar{n}_F^0(\mathbf{r})$ is essentially constant for large ζ, as shown in Fig. 3(c). While the same qualitative evolution occurs at all sites in the network, $\bar{n}_F^0(\mathbf{r})$ in the limit $\zeta \to \infty$ depends on the location inside the network, as shown in Fig. 3(d). At the same time, $\text{Im}G^r(\mathbf{r},\omega)$ becomes nearly independent of energy

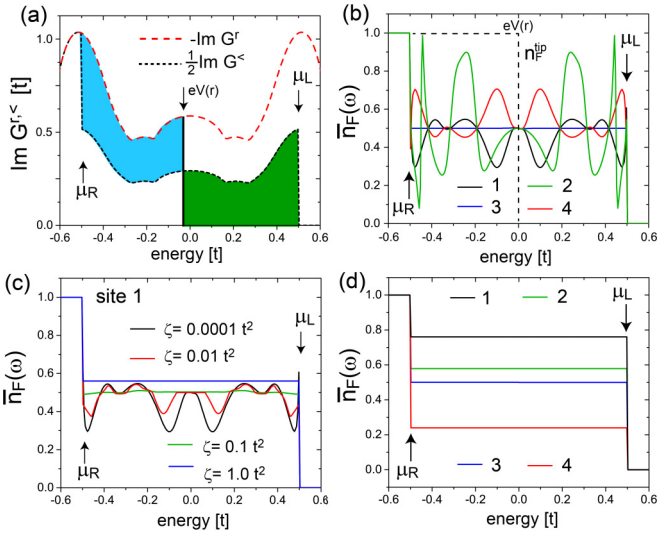

FIG. 3. (a) $\text{Im}G^{r,<}$ at site 5 [see Fig. 1(b)] for $\mu_{L,R} = \pm 0.5t$ and $\zeta = 0.1t^2$. (b) $\bar{n}_F$ for $\mu_{L,R} = \pm 0.5t$ and $\zeta = 0.000\,1t^2$ at sites 1–4 in Fig. 1(b) and n_F^{tip} (dashed line). (c) Evolution of $\bar{n}_F$ with increasing ζ at site 1. (d) $\bar{n}_F$ in the large ζ limit ($\zeta = 100t^2$).

for $\mu_R < \omega < \mu_L$, such that the graphic solution for finding $V(\mathbf{r})$ discussed above now allows us to directly relate $\bar{n}_F^0$ and $\mu_e(\mathbf{r})$ via

$$\mu_e(\mathbf{r}) = \mu_R + \bar{n}_F^0(\mathbf{r})(\mu_L - \mu_R). \tag{3}$$

The above discussion shows that the spatial dependence of $\mu_e(\mathbf{r})$ is a truly nonequilibrium phenomenon, as it is spatially constant and equal to the network's uniform chemical potential in equilibrium where $\mu_{L,R} = 0$. $\mu_e(\mathbf{r})$ should also not be interpreted as representing a local equilibrium value, since the strong dependence of $\bar{n}_F$ on energy [see Figs. 3(b) and 3(c)] implies that $\bar{n}_F$ cannot be described by an equilibrium Fermi distribution function with a renormalized temperature or chemical potential.

We next investigate the behavior of μ_e around defects, and to this end consider a network connected to wide leads (see Fig. 4). In Figs. 4(a) and 4(b) we present the spatial form of $\mu_e(\mathbf{r})$ and corresponding $I_{\mathbf{r},\mathbf{r}'}$ near the ballistic quantum limit for a wide-lead network without a defect. The current shows a very weak variation in magnitude inside the network, with the largest changes occurring along the edges, while the potential exhibits a variation across the network that is much more uniform than in the narrow-lead case [see Fig. 2(a)]. The addition of a nonmagnetic defect in the center of the network leads to significant changes in $\mu_e(\mathbf{r})$ and $I_{\mathbf{r},\mathbf{r}'}$ [see Figs. 4(c) and 4(d)] that extend throughout the entire network and are predominantly confined to the lattice diagonal. This is a direct consequence of the Fermi surface's large degree of nesting [see Fig. 1(c)] and a Fermi velocity along the diagonal direction in the Brillouin zone. With increasing ζ, the effects induced by the defect in $\mu_e(\mathbf{r})$ and $I_{\mathbf{r},\mathbf{r}'}$ are reduced in amplitude [see Figs. 4(e) and 4(f)] and become spatially more confined to the immediate vicinity of the defect, indicating the crossover from nonlocal transport in the quantum limit to local transport in the classical limit [29].

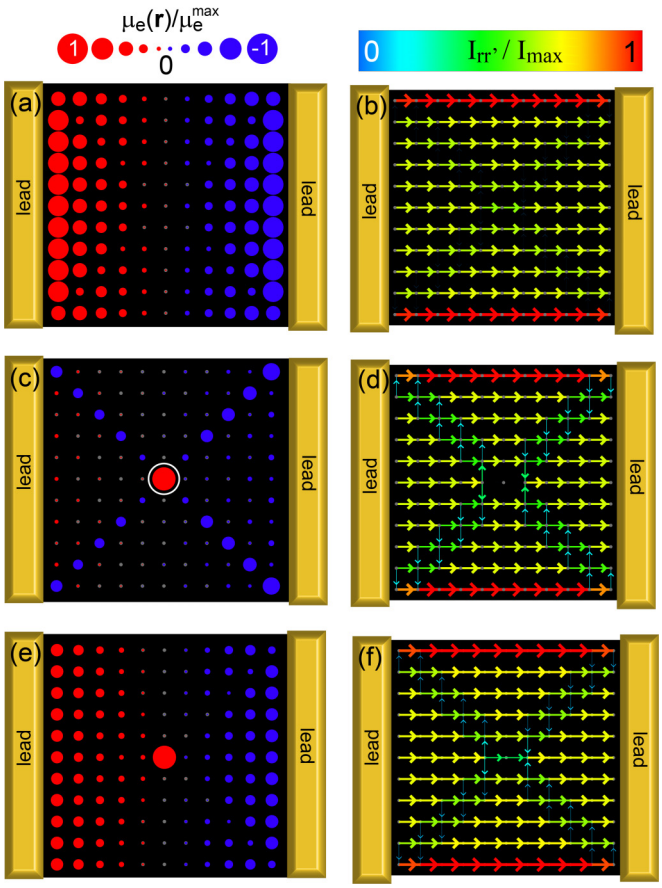

FIG. 4. Network connected to wide leads with $\mu_{L,R} = \pm 0.05t$. (a) Normalized $\mu_e(\mathbf{r})$ and (b) $I_{\mathbf{r},\mathbf{r}'}$ for $\zeta = 0.01t^2$. (c)–(f) Normalized $\mu_e(\mathbf{r})$ and $I_{\mathbf{r},\mathbf{r}'}$ for a network with a defect of $U_0 = t$ located at the center [as indicated by an open white circle in (c)] and (c, d) $\zeta = 0.01t^2$, and (e, f) $\zeta = 0.2t^2$. $\mu_e(\mathbf{r})$ at the defect site in (c) has been divided by a factor of 3 for clarity.

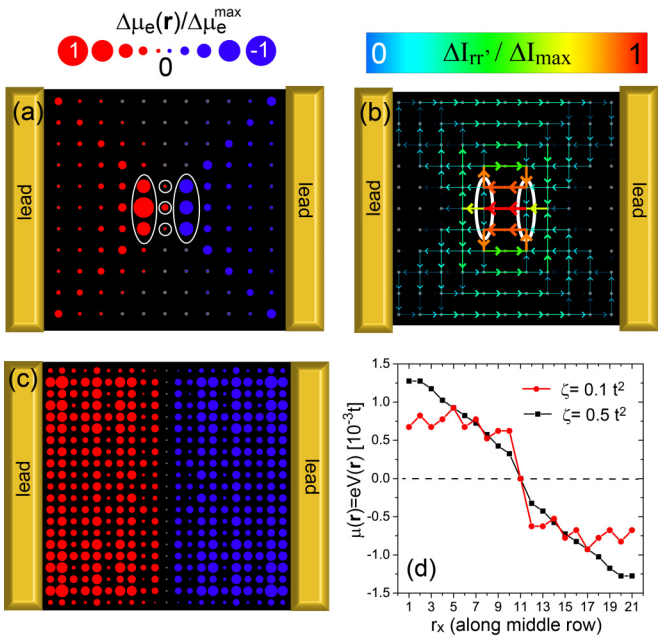

FIG. 5. Network connected to wide leads with three defects [as indicated by open white circles in (a)] of scattering strength $U_0 = 3t$. (a) Normalized $\Delta\mu_e(\mathbf{r})$ and (b) $\Delta I_{\mathbf{r},\mathbf{r}'}$ for $\zeta = 0.5t^2$. (c) Normalized $\mu_e(\mathbf{r})$ for a network with $N_x = N_y = 21$ and different chemical potentials in the left ($\mu = +t$) and right ($\mu = -t$) parts of the network, $\mu_{L,R} = \pm 0.01t$ and $\zeta = 0.1t^2$. (d) Line cut of $\mu_e(\mathbf{r})$ along the center row of (c).

To visualize the formation of a residual resistivity dipole [19,20], we present in Figs. 5(a) and 5(b) the changes induced in the electrochemical potential $\Delta\mu_e(\mathbf{r})$ and in the spatial current pattern $\Delta I_{\mathbf{r},\mathbf{r}'}$, respectively, by placing three defects [see small white circles in Fig. 5(a)] in the center of the network.

The spatial form of $\Delta\mu_e(\mathbf{r})$ reveals the dipole nature of the induced changes, with an enhancement (suppression) of $\mu_e(\mathbf{r})$ towards the lead with the higher (lower) chemical potential, thus demonstrating the existence of a defect-induced residual resistivity dipole. Interestingly enough, the spatial form of $\Delta I_{\mathbf{r},\mathbf{r}'}$ [see Fig. 5(b)] is that of field lines associated with the presence of a dipole. This becomes particulary evident when we indicate the regions with the largest $\Delta\mu_e(\mathbf{r})$ (see white ellipses next to the defects) in the plot of $\Delta I_{\mathbf{r},\mathbf{r}'}$. We therefore conclude that the relation between the defect-induced changes in $\mu_e(\mathbf{r})$ and $I_{\mathbf{r},\mathbf{r}'}$ is that of dipole charges and their associated field lines. Finally, to explore the form of $\mu_e(\mathbf{r})$ near interfaces or step edges, we apply different chemical potentials to the left ($\mu = +t$) and right ($\mu = -t$) parts of a network. The resulting $\mu_e(\mathbf{r})$ shown in Figs. 5(c) and 5(d) exhibit not only, as expected, a sharp drop at the center of the network where the change in chemical potential occurs, but also spatial oscillations that extend all the way back to the leads. This is reminiscent of the spatial oscillations found near step edges in [18]. With increasing ζ, this sharp drop is smoothed out, leading to more gradual variations of $\mu_e(\mathbf{r})$ across the network [Fig. 5(d)].

IV. CONCLUSIONS

In summary, we identified the spatial relation between the electrochemical potential and the current patterns over the entire range from quantum to classical transport. These two quantities show similar spatial patterns near the quantum limit but are related by Ohm's law only in the classical regime. We showed that defects induce a Landauer residual resistivity dipole in $\mu_e(\mathbf{r})$, with the spatial form of the concomitant $\Delta I_{\mathbf{r},\mathbf{r}'}$ representing the field lines associated with the dipole. A similar approach might be used to investigate the relation between heat currents and local temperature measurements out of equilibrium [32,33].

ACKNOWLEDGMENTS

We would like to thank M. Beasley, M. Graf, and M. Wenderoth for stimulating discussions. This work was supported by the US Department of Energy, Office of Science, Basic Energy Sciences, under Award No. DE-FG02-05ER46225.

[1] R. Crook, C. G. Smith, M. Y. Simmons, and D. A. Ritchie, Phys. Rev. B **62**, 5174 (2000).
[2] R. Crook, C. G. Smith, C. H. W. Barnes, M. Y. Simmons, and D. A. Ritchie, J. Phys.: Condens. Matter **12**, L167 (2000).
[3] M. A. Eriksson, R. G. Beck, M. Topinka, J. A. Katine, and R. M. Westervelt, Appl. Phys. Lett. **69**, 671 (1996).
[4] M. A. Topinka, B. J. LeRoy, S. E. J. Shaw, E. J. Heller, R. M. Westervelt, K. D. Maranowski, and A. C. Gossard, Science **289**, 2323 (2000).
[5] M. A. Topinka, B. J. LeRoy, R. M. Westervelt, S. E. J. Shaw, R. Fleischmann, E. J. Heller, K. D. Maranowski, and A. C. Gossard, Nature (London) **410**, 183 (2001).
[6] K. E. Aidala, R. E. Parrott, T. Kramer, E. J. Heller, R. M. Westervelt, M. P. Hanson, and A. C. Gossard, Nat. Phys. **3**, 464 (2007).
[7] M. P. Jura, M. A. Topinka, L. Urban, A. Yazdani, H. Shtrikman, L. N. Pfeiffer, K. W. West, and D. Goldhaber-Gordon, Nat. Phys. **3**, 841 (2007).
[8] B. Hackens, F. Martins, T. Ouisse, H. Sellier, S. Bollaert, X. Wallart, A. Cappy, J. Chevrier, V. Bayot, and S. Huant, Nat. Phys. **2**, 826 (2006).
[9] F. Martins, B. Hackens, M. G. Pala, T. Ouisse, H. Sellier, X. Wallart, S. Bollaert, A. Cappy, J. Chevrier, V. Bayot, and S. Huant, Phys. Rev. Lett. **99**, 136807 (2007).
[10] B. Hackens, F. Martins, S. Faniel, C. A. Dutu, H. Sellier, S. Huant, M. Pala, L. Desplanque, X. Wallart, and V. Bayot, Nat. Commun. **1**, 39 (2010).
[11] P. Muralt and D. W. Pohl, Appl. Phys. Lett. **48**, 514 (1986).
[12] B. G. Briner, R. M. Feenstra, T. P. Chin, and J. M. Woodall, Phys. Rev. B **54**, R5283(R) (1996).
[13] C. S. Chu and R. S. Sorbello, Phys. Rev. B **42**, 4928 (1990).
[14] W. Wang and M. R. Beasley, arXiv:1007.1512v2.
[15] J. Homoth, M. Wenderoth, T. Druga, L. Winking, R. G. Ulbrich, C. A. Bobisch, B. Weyers, A. Bannani, E. Zubkov, A. M. Bernhart, M. R. Kaspers, and R. Möller, Nano Lett. **9**, 1588 (2009).
[16] S.-H. Ji, J. B. Hannon, R. M. Tromp, V. Perebeinos, J. Tersoff, and F. M. Ross, Nat. Mater. **11**, 114 (2012).
[17] W. G. Wang, K. Munakata, M. Rozler, and M. R. Beasley, Phys. Rev. Lett. **110**, 236802 (2013).
[18] P. Willke, T. Druga, R. G. Ulbrich, M. A. Schneider, and M. Wenderoth, Nat. Commun. **6**, 6399 (2015).
[19] R. Landauer, IBM J. Res. Dev. **1**, 223 (1957).
[20] R. Landauer, Z. Phys. B: Condens. Matter Quanta **21**, 247 (1975).
[21] L. V. Keldysh, Sov. Phys. JETP **20**, 1018 (1965).
[22] J. Rammer and H. Smith, Rev. Mod. Phys. **58**, 323 (1986).
[23] C. Caroli, R. Combesco, P. Nozieres, and D. Saintjam, J. Phys. C: Solid State Phys. **4**, 916 (1971).
[24] A. Cresti, R. Farchioni, G. Grosso, and G. P. Parravicini, Phys. Rev. B **68**, 075306 (2003).
[25] T. N. Todorov, Philos. Mag. B **79**, 1577 (1999).
[26] T. Can, H. Dai, and D. K. Morr, Phys. Rev. B **85**, 195459 (2012).
[27] T. Can and D. K. Morr, Phys. Rev. Lett. **110**, 086802 (2013).
[28] K. H. Bevan, Nanotechnology **25**, 415701 (2014).
[29] D. K. Morr, Contemp. Phys. **57**, 19 (2016).
[30] Z. Bihary and M. A. Ratner, Phys. Rev. B **72**, 115439 (2005).
[31] F. Y. Wu, J. Phys. A: Math. Gen. **37**, 6653 (2004).
[32] J. P. Bergfield, M. A. Ratner, C. A. Stafford, and M. Di Ventra, Phys. Rev. B **91**, 125407 (2015).
[33] A. Shastry and C. A. Stafford, Phys. Rev. B **94**, 155433 (2016).